Journal of Molecular Catalysis A: Chemical 295 (2008) 57–67

Contents lists available at ScienceDirect

Journal of Molecular Catalysis A: Chemical

journal homepage: www.elsevier.com/locate/molcata

Palladium within ionic liquid functionalized mesoporous silica SBA-15 and its catalytic application in room-temperature Suzuki coupling reaction

Peng Han[a,b], Hongming Zhang[b], Xuepeng Qiu[b], Xiangling Ji[a,*], Lianxun Gao[a,b,**]

[a] State Key Laboratory of Polymer Physics and Chemistry, Changchun Institute of Applied Chemistry, Chinese Academy of Sciences, Graduate School of the Chinese Academy of Sciences, 5625 Renmin Street, Changchun 130022, People's Republic of China
[b] Laboratory of Polymer Engineering, Changchun Institute of Applied Chemistry, Chinese Academy of Sciences, Graduate School of the Chinese Academy of Sciences, 5625 Renmin Street, Changchun 130022, People's Republic of China

ARTICLE INFO

Article history:
Received 3 January 2008
Received in revised form 24 August 2008
Accepted 30 August 2008
Available online 5 September 2008

Keywords:
Palladium
Mesoporous
Ionic liquid
Catalysis
Coupling
Suzuki
Room temperature

ABSTRACT

Initially, pore walls of mesoporous silica SBA-15 with template were modified with chlorotrimethylsilane. Then imidazolium salts were similarly incorporated covalently in the inner pore walls of mesoporous silica SBA-15 albeit without the template. Finally, palladium salts were introduced into the pore channels of the previously processed mesoporous silica *via* electrostatic interaction. The resulting palladium catalysts demonstrated exceptional activity for the room-temperature Suzuki coupling reaction in aqueous-organic mixed solvents and good recycling ability for at least 4–6 times. The turnover frequency of resulting catalysts could reach up to 84,000 h^{-1} at 50 °C. The corresponding samples were analyzed with solid-state NMR, FT-IR, XRD, nitrogen adsorption–desorption isotherms, TEM and XPS techniques. In addition, agglomeration of palladium catalyst in the Suzuki coupling reaction can be effectively controlled due to the stabilizing effect of the imidazulium salt and confinement of mesoporous walls.

1. Introduction

Palladium as a catalyst has played an important role in organic synthesis over the past decades [1]. Palladium-catalyzed coupling reactions offer an abundance of possibilities to asymmetric carbon–carbon bond formation such as the Mizoroki-Heck [2,3], Suzuki-Miyaura [4,5], Sonogashira [6], and Stille [7] coupling reactions. On the other hand, palladium catalysts are also exploited in carbon–nitrogen bond formation such as the Buchwald-Hartwig coupling reactions [8,9]. Palladium catalysts with phosphines ligand [10,11], carbenes ligand [12,13], palladacycle [14], and other coordinates have likewise led to the activation of weak leaving groups such as chloride, have also led to the exhibition of higher TON (turnover number) and reaction rates, and have improved the lifespan and stability of the reactions with water or under air at room temperature. New techniques as well have been developed, such as microwave-assisted heating technology [15]. However, two factors limit the commercialization of new catalysts. One is an additional separation step required to remove the homogeneous catalyst from the product. Another is recycling the expensive transition metal and ligand. Fortunately, a few strategies overcome the above drawbacks, for example, heterogeneous catalysts [16] and two-phase catalysis can make use of various solvent combinations, fluorinated solvents, supercritical fluids, dendrimers, and ionic liquids [17].

Heterogeneous palladium catalysis has been investigated extensively for the Suzuki cross-coupling reaction. Different supporting materials and approaches have been exploited for the immobilization of palladium precursors which include palladium (II) exchanged sepiolite clay [18] and NaY zeolite [19], palladium containing perovskite [20], carbon-supported palladium nanoparticles [21,22], hydroxyapatite supported palladium complexes [23], poly-HIPE (i.e., a porous polymer obtained by the polymerization of a high internal phase emulsion) supported palladium nanoparticles [24], subnanometer palladium clusters immobilized on random copolymer micelles [25], and palladium immobilized on mesoporous SiO_2 [26–30]. Recently, the palladium catalysts for the

* Corresponding author. Tel.: +86 431 8526 2876/2203; fax: +86 431 85685653.
** Corresponding author at: State Key Laboratory of Polymer Physics and Chemistry, Changchun Institute of Applied Chemistry, Chinese Academy of Sciences, 5625 Renmin Street, Changchun 130022, People's Republic of China.
E-mail addresses: xlji@ciac.jl.cn (X. Ji), lxgao@ciac.jl.cn (L. Gao).

1381-1169/$ – see front matter © 2008 Elsevier B.V. All rights reserved.
doi:10.1016/j.molcata.2008.08.016

room-temperature Suzuki coupling reaction have been widely investigated, such as ligand-free palladium catalysts [31] and commercialized Pd/C catalysts [22].

As reported in the literature, ionic liquids often result in a significant improvement in catalytic performance [32–34]. However, the wide use of industrial ionic liquids is hindered primarily by their high cost, limited information on their physico-chemical properties, separating behavior, biodegradability, and ecotoxicology. Therefore, supported ionic liquids as an alternative approach were studied in recent years [35–41]. Hagiwara et al. developed highly efficient Suzuki coupling of aryl halides with arylboronic acids in 50% aqueous ethanol and employing $Pd(OAc)_2$ immobilized in diethylaminopropylated alumina pores with the aid of an ionic liquid ([bmim][PF_6]) without a phosphine ligand at room temperature in a short period of time [42]. However, the ionic liquids covalently bonded to the inorganic porous oxides which exhibit better thermal and mechanical properties than that of impregnation, and minimize the consumption of ionic liquids in catalytic reactions. Among the inorganic porous oxides, highly ordered mesoporous silica could be an outstanding carrier due to its large specific surface area, highly ordered pore structure, and inert environment [43,44]. Thiot et al., meanwhile, have shown that polyionic gels represent a feasible alternative to ionic liquids as reaction media for recyclable heterogeneous catalytic systems [45]. These polyionic gels display an efficient metal soaking ability, which rely on strong noncovalent interactions between metal and ions within the gel. Similarly, they provide favorable and stabilizing environments for the generation of heterogeneous metal-based catalytic systems. Pd-soaked polyionic gels have actually been used in Suzuki coupling reaction, while Rh-soaked polyionic gels have been used in hydrosilylation of phenylacetylene with diethoxylmethylsilane.

In this study, taking into account the advantage of mesoporous silica, we present the option of covalent immobilization of imidazolium salts inside the channel of mesoporous silica SBA-15. The resultant materials with highly ionized surfaces and large surface areas are suitable as efficient scavengers of novel metal salts and as substances for supported catalyst preparation. The palladium-based supported catalysts are then prepared and their catalytic performance for the Suzuki cross-coupling reaction at room temperature investigated.

2. Experimental

2.1. Catalyst preparation

2.1.1. Synthesis of N-3-(3-triethoxysilyl propyl)-3-methyl imidazolium chloride

N-3-(3-triethoxysilyl propyl)-3-methyl imidazolium chloride was synthesized through 1-methylimidazole and (3-choropropyl)-triethoxysilane in dried toluene refluxed for 24 h under argon atmosphere. Then toluene was removed from the solution under reduced pressure. The remaining liquid was washed with diethyl ester 4 times and dried in a vacuum oven for 10 h. Finally, white, wax-like solid was obtained. The product was verified using ^{1}H NMR and ^{13}C NMR analysis. ^{1}H NMR δ_H (ppm, 300 MHz, DMSO-d6): 9.32 (s, 1H), 7.82 (t, J = 1.5 Hz, 1H), 7.76 (t, J = 1.5 Hz, 1H), 4.16 (t, 2H, CH_2), 3.78 (s, 3H, CH_3), 3.87 (s, 3H, CH_3), 3.74 (s, 6H, CH_2), 1.81 (m, 2H, CH_2), 1.13 (t, 9H, CH_3), 0.51 (m, 2H, CH_2); ^{13}C NMR δ_C (ppm, 75.4 MHz, DMSO-d6): 136.2, 123.5, 122.1, 57.8, 50.9, 39.5, 35.6, 23.6, 18.1, 6.6.

2.1.2. Preparation of mesoporous silica SBA-15

Mesoporous silica SBA-15 samples were prepared according to the previously mentioned study in literature [46]. A typical procedure was described as follows: 9 g of triblock copolymer Pluronic P123 was dissolved in a solution of 70 mL of deionized water, then 150 g of 2 M HCl at 35 °C was added to the above solution under stirring. Afterwards, 20 g of TEOS was added into the above solution. The resulting mixture was stirred at 35 °C for 24 h, and then aged at 80 °C for 24 h. Finally, the white powder samples were acquired.

2.1.3. Immobilization of palladium salt in the pore channels of imidazolium-functionalized mesoporous silica SBA-15 (Pd-M-T-S)

In this section, mesoporous SBA-15 samples were firstly stirred with chlorotrimethylsilane before the template P123 was removed. The hydroxyls outside of the pore walls were protected in advance. Then the template P123 was removed with ethanol in a Soxhlet extractor at 100 °C for 24 h and then dried in vacuum. The obtained materials were designated as TMS-S. Then, samples of TMS-S were refluxed with *N*-3-(3-triethoxysilyl propyl)-3-methyl imidazolium chloride in dry toluene for 24 h under argon atmosphere. After filtration and drying, the white powder samples were collected. The obtained materials were designated as T-M-S. Finally, the adsorption of palladium salt was performed by ultrasonication of 1 g imidazolium salts-functionalized mesoporous silica with 20 mL DMF solution of $PdCl_2$ (0.2 M) for 30 min at room temperature. After filtration, washing and drying, the yellow powder was collected. We designated it as Pd-M-T-S. The process has been illustrated in Fig. 1. For comparison, palladium salts were also immobilized on unmodified mesoporous SBA-15 *via* wet impregnation. For example, a suspension of 5 mL DMF solution of $PdCl_2$ (0.2 M) and 0.5 g of unmodified mesoporous SBA-15 in 20 mL of acetone were stirred for 24 h. The solvents were removed by rotary evaporation. The resulting samples were dried in vacuum at 100 °C. The acquired yellow powder was designated as Pd (II)/SBA-15.

2.2. Characterization

^{13}C- and ^{29}Si-cross polarization magic-angle spinning (CP-MAS) NMR were recorded on a 400 MHz Bruker Avance instrument. FT-IR spectra were recorded on a Boi-Rad FTS135 infrared spectrometer. Low-angle X-ray diffraction (XRD) patterns were recorded on a D8 X-ray Reflector with Cu Kα radiation at 40 kV and 40 mA. Typically, the data were collected in the range of $0.5^\circ < 2\theta < 3^\circ$ with a step size of 0.01° and a count time of 1 s per step. Wide-angled XRD patterns were recorded with PW1700 X. The data were then collected in the range of $10^\circ < 2\theta < 80^\circ$ with a step size of 0.1° and a count time of 1 s per step. Transmission electron microscope (TEM) examination was subsequently carried out using a JEOL-1011 electron microscope with an accelerating voltage of 100 kV. The samples were prepared by dispersing the silica powder in ethanol and dropping on copper grids. Nitrogen adsorption–desorption isotherms at 77 K for mesoporous silica particles and modified silica samples were next obtained using a NOVA1000. The specific surface area was calculated employing the multiple-point the Brunauer-Emmett-Teller (BET) method. The pore size distribution curves were computed using the Barrett-Joyner-Halenda (BJH) method. This was followed by the verification of the content of palladium in the samples by inductively coupled plasma-atomic emission spectroscopy (ICP-AES) and elemental analysis finally. Meanwhile, X-ray photoelectron spectra (XPS) were measured with VG ESCALAB MK (VG Company, UK) at room temperature using a Mg Kα X-ray source ($h\nu$ = 1253.6 eV) at 14 kV and 20 mA. Gas chromatograph (GC) analyses were performed on a Shimadzu G-2010A instrument. Lastly, ^{1}H and ^{13}C NMR were recorded on a 300 MHz Bruker Avance instrument, with $CDCl_3$ or DMSO-d6 as the solvent and TMS as the internal standard.

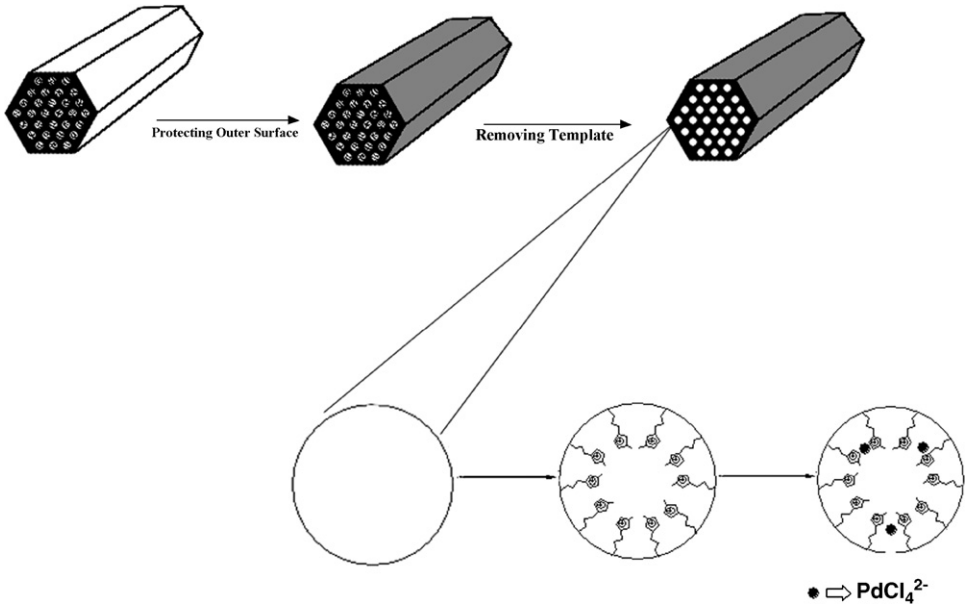

Fig. 1. Illustration of the procedure for immobilization of $PdCl_4^{2-}$ in imidazolium-functionalized mesoporous silica SBA-15.

2.3. Procedure for Suzuki cross-coupling reaction

2.3.1. Suzuki cross-coupling reaction between aryl halide with arylboronic acid

A typical experiment for the Suzuki coupling reaction between aryl halide with arylboronic acid was carried out in a 50 mL round-bottomed flask with 20 mL of solvents composed of 2.0 mmol of aryl halides, 2.2 mmol of arylboronic acids, and 6.0 mmol of bases in the presence of palladium catalysts. These were magnetically stirred at room temperature. After this procedure, the mixture was diluted with ethyl ether. The used catalysts were separated by filtration. The filtrate was separated into two layers, and the aqueous layer was extracted with ethyl ether several times. The combined organic layers were dried over $MgSO_4$ and were analyzed by gas chromatograph.

2.3.2. Suzuki cross-coupling reaction between dihaloaromatic with arylboronic acid

Another typical experiment for the Suzuki coupling reaction was carried out in a 50 mL round-bottomed flask with 20 mL of $EtOH/H_2O$ (v/v = 1:1) co-solvent made up of 1.0 mmol of dihaloaromatic, 2.2 mmol of arylboronic acids, and 6.0 mmol of K_2CO_3 in the presence of 3.1 wt.% Pd-M-T-S (Pd/dihaloaromatic = 1/500 in molar ratio). These were magnetically stirred at room temperature. After this procedure, the mixture was diluted with CH_2Cl_2. The used catalysts were separated by filtration. The filtrate afterwards was separated into two layers and the aqueous layer was extracted with CH_2Cl_2 several times. The combined organic layers were dried over $MgSO_4$, filtered, and evaporated to dryness. Yield was determined by ^1H NMR spectroscopy.

2.3.3. Recovery and reuse of Pd-M-T-S

The recycling experiment for the Suzuki coupling reaction was carried out in a 250 mL round-bottomed flask with 100 mL of $EtOH/H_2O$ (v/v = 1:1) co-solvent composed of 20 mmol of *p*-bromoanisole, 22 mmol of phenylboronic acids, and 60 mmol of K_2CO_3 in the presence of 3.1 wt.% Pd-M-T-S (Pd/*p*-bromoanisole = 1/1000 in molar ratio). These were magnetically stirred at room temperature. After this procedure, the mixture was diluted with ethyl ether. The used catalysts were separated by filtration, washed with deionized water and acetone, and dried for the next run. The filtrate was separated into two layers and the aqueous layer was extracted with ethyl ether several times. The combined organic layers were dried over $MgSO_4$ and analyzed by GC. The dried catalysts were weighed and reused in the next run; proportional amounts of reactants were added to keep the substrate-to-catalyst and the solvent-to-catalyst ratios constant throughout the series of reuses.

3. Results and discussion

3.1. Characterization of catalyst

The structure of the organic functionality was proved through comparing the liquid-state ^{13}C NMR spectrum of *N*-3-(3-triethoxysilyl propyl)-3-methyl imidazolium chloride (Fig. 2A) with the solid-state ^{13}C CP-MAS NMR of M-T-S (Fig. 2B). The assignments of ^{13}C resonances in solution were based on the observed chemical shifts (see Table 1). The shifts obtained in solid-state NMR spectra of M-T-S, which are also listed in Table 1, match well with the solution data, and thus confirm the presence of the imidazolium groups on the silica surface [47].

The concentration of functional groups in M-T-S was measured from the relative intensities of T^n and Q^n silicon groups observed by ^{29}Si CP-MAS NMR spectrum. Q^2, Q^3 and Q^4 represent silicon atoms (denoted as Si*) in $(HO)_2Si^*(OSi)_2$, $HOSi^*(OSi)_3$ and $Si^*(OSi)_4$ silicate species, respectively. T^2 and T^3 represent silicon atoms (denoted as Si*) in $RSi^*(OH)(OSi)_2$ and $RSi^*(OSi)_3$ species, where R is the organic functional group. A peak at −110 to −111 ppm comes from Q^4, the peak at −102 to −103 ppm comes from Q^3, the peak at −92 to −93 ppm comes from Q^2 and the other peaks are related to T^3 and T^4 (see Fig. 3). The presence of the T units ($T^2 + T^3$) further suggests the incorporation of organic groups within the mesoporous silicas. By deconvolution and integration of the ^{29}Si spectrum, the following molecular formula was obtained for M-T-S: $(SiO_2)_{100}(H_2O)_{12}(C_7H_{12}N_2Cl)_{13}$. The concentration of imidazolium groups is calculated as being 1.6 mmol g^{-1} and the surface densities of organic groups can be estimated to be 2.1 nm^{-2}.

The presence of the imidazolium functional group in the catalytic materials was also confirmed from the FT-IR spectrum (Fig. 4).

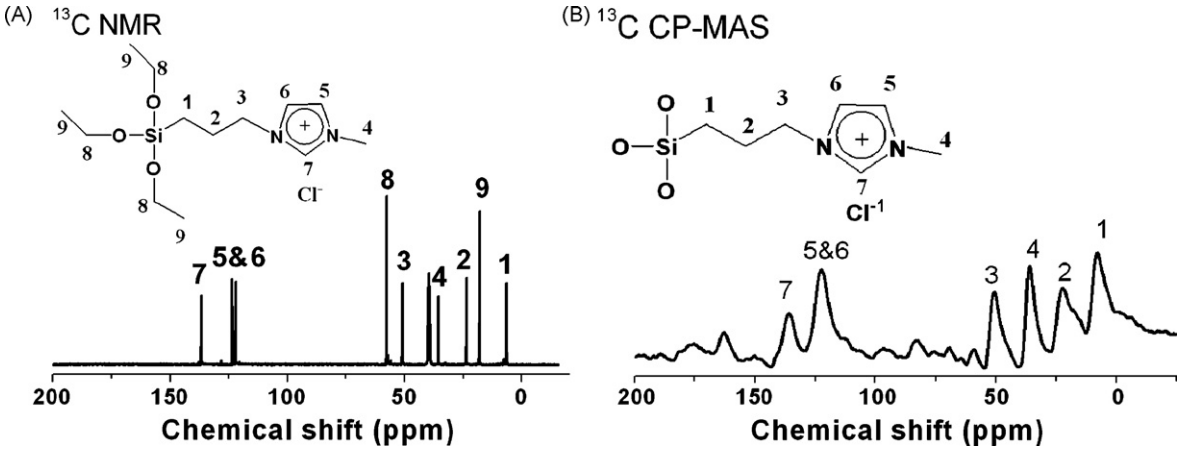

Fig. 2. (A) ^{13}C NMR spectrum of *N*-3-(3-triethoxysilyl propyl)-3-methyl imidazolium chloride in DMSO-d6 solution. (B) ^{13}C CP-MAS NMR spectrum of M-T-S.

Table 1
^{13}C chemical shifts for *N*-3-(3-triethoxysilyl propyl)-3-methyl imidazolium chloride and M-T-S (ppm)

Sample	Solvent	C1	C2	C3	C4	C5	C6	C7	C8	C9
MIM-TES	DMSO-d6	6.6	23.6	50.9	35.6	123.5	122.1	136.2	57.8	18.1
M-T-S	Solid-state	7.8	22.3	50.6	35.9	122.5	136	–	–	

FT-IR spectrum of M-T-S (Fig. 4b) exhibit three bands at 1574, 1462 and 619 cm^{-1}, assigned to the C–H bending vibration of imidazolium groups, the propyl group and methyl group respectively. The three peaks are not observed in the spectrum of the pure SBA-15 (Fig. 4a). Pure SBA-15 materials show characteristic bands at 3470 cm^{-1} from the Si–OH stretching vibration and 1638 cm^{-1} the O–H stretching vibration and bands at 1081, 951 798, 565 and 460 cm^{-1} due to the Si–O stretching vibration. A very intense and broad band at a high frequency region between 3700 and 3200 cm^{-1} implies the presence hydrogen bonding in the mesoporous silica [48].

Powder low-angle XRD patterns for the resultant materials are shown in Fig. 5. All samples exhibit one intense peak at 0.81–0.82° along with two weak peaks at 1.41–1.42° and 1.61–1.63°, which correspond to 100, 110, and 200 reflections. These results suggest the presence of periodic arrangement of channels in a hexagonal geometry. The pure SBA-15 shows a diffraction peak at a 2θ of 0.81°, which corresponds to its *d*-spacing of 10.9 nm. We likewise noted that the intensities of the diffraction peaks become weak and the ordered pore structure are remained after modification on the surface of mesoporous silica SBA-15.

TEM images for Pd-M-T-S (Fig. 6) clearly show two dimensional hexagonal symmetry structures. It indicates the remaining overall structure after a series of modifications on the surface of meso-

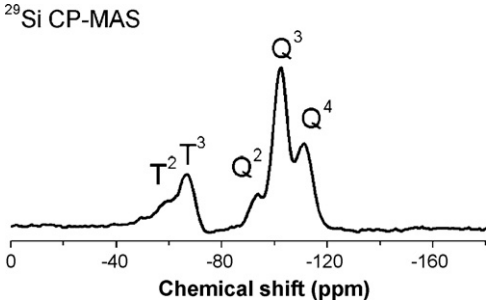

Fig. 3. ^{29}Si CP-MAS NMR spectrum of M-T-S.

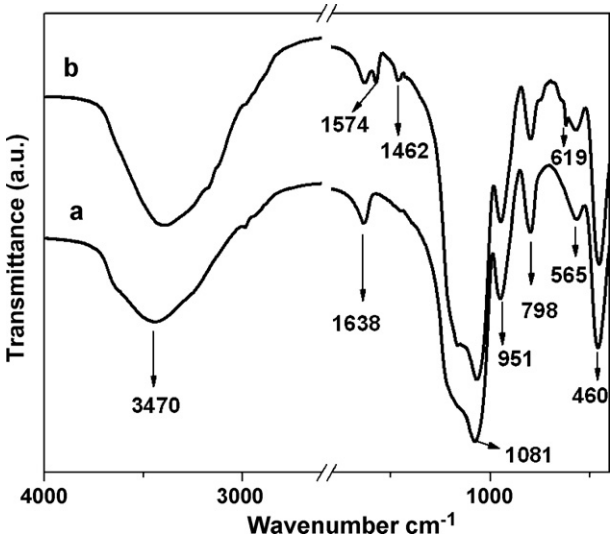

Fig. 4. FT-IR spectra of pure SBA-15 (a) and M-T-S (b).

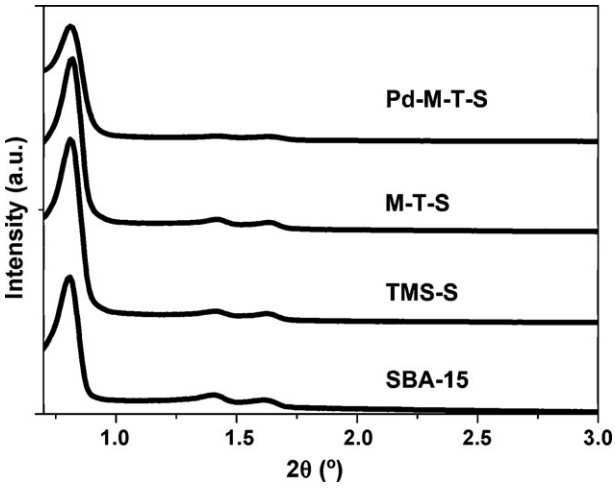

Fig. 5. Low-angle XRD patterns for bare mesoporous silica SBA-15, trimethylsilane modified the outer surface of mesoporous SBA-15 (TMS-S), imidazolium salts functionalized the TMS-S (M-T-S) and palladium salt loaded on the M-T-S (Pd-M-T-S).

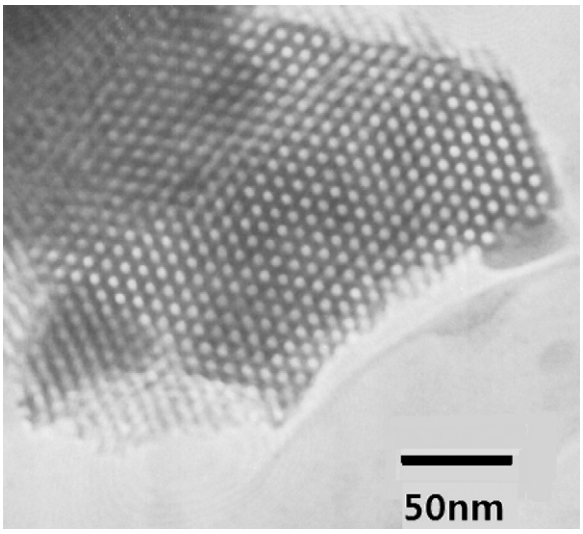

Fig. 6. TEM image of Pd-M-T-S; scale bar = 50 nm.

porous silica. The nitrogen adsorption–desorption isotherms at 77 K for the samples are shown in Fig. 7A and the corresponding pore size distribution curves can be seen in Fig. 7B. The BET surface areas decrease from 803 to 599, 509, 461 $m^2\ g^{-1}$ for pure SBA-15, TMS-S, M-T-S, and Pd-M-T-S, respectively. Meanwhile, the average pore sizes are 54.1, 64.7, 67, 65.8 Å. The pore volume also decreases from 1.09 to 0.97, 0.84, 0.77 $cm^3\ g^{-1}$ for pure SBA-15, TMS-S, M-T-S and Pd-M-T-S samples, respectively.

The content of palladium in the samples was confirmed finally by ICP-AES elemental analysis. The weight percentages of palladium are 3.1 wt.% (0.28 mmol g^{-1}), 2.0 wt.% (0.18 mmol g^{-1}) for Pd-M-T-S, Pd (II)/SBA-15, respectively.

3.2. Optimization of reacting condition

In this section, we firstly investigated the corresponding parameters for the Suzuki cross-coupling reaction. It includes different solvents and bases for the room-temperature Suzuki reaction, of *p*-bromoanisole, and phenylboronic acid in the presence of 3.1 wt.% Pd-M-T-S. The molar ratio of Pd/*p*-bromoanisole was set at 1/1000 for the Suzuki coupling reaction. The single solvent such as dioxane, toluene, DMF, iPrOH, EtOH, and H_2O gave low yields ranging from 0 to 53% as illustrated in Table 2, entries 1–6. When we adopted the organic/aqueous co-solvent, satisfactory results were obtained. They afforded high yields of 89–97% as shown in Table 2, entries 7–9. The merit of the co-solvent is attributed to the good solubility of the organic reactants and the inorganic base. We next tested the influence of different volume ratios of EtOH/H_2O as a solvent under the Suzuki reaction at room temperature. They afforded yields of 42–97%, as demonstrated in Table 2, entries 9–13. Evidently, the optional volume ratio should be set at 1:1.

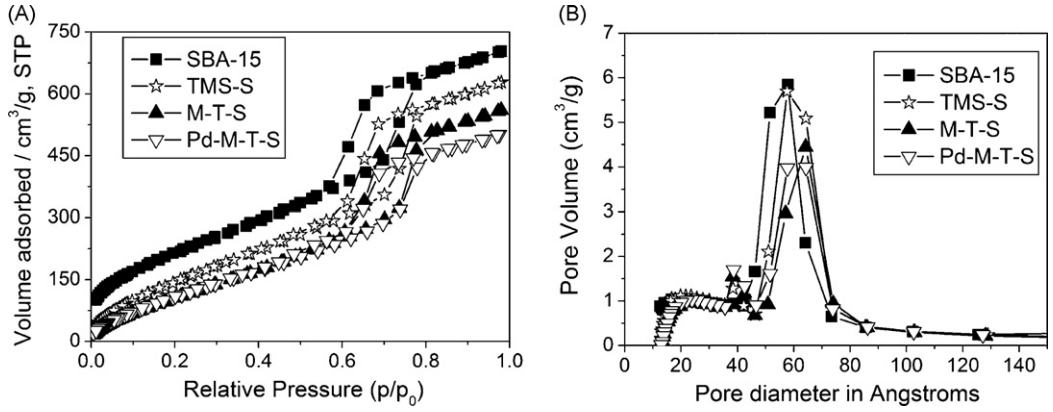

Fig. 7. (A) Nitrogen adsorption–desorption isotherms for the resulting materials; (B) corresponding pore size distribution by BJH model.

Table 2
Effect of solvents and temperature for the Suzuki reaction of *p*-bromoanisole and phenylboronic acid

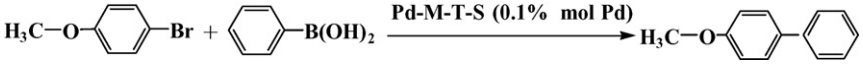

Entry	Solvent system	Base	Temperature	Time (h)	Yield (%)[b]
1[a]	Dioxane	K_2CO_3	RT	1	12
2[a]	Toluene	K_2CO_3	RT	1	5
3[a]	DMF	K_2CO_3	RT	1	53
4[a]	iPrOH	K_2CO_3	RT	1	46
5[a]	EtOH	K_2CO_3	RT	1	34
6[a]	H_2O	K_2CO_3	RT	1	0
7[a]	DMF/H_2O (v/v = 1:1)	K_2CO_3	RT	1	89
8[a]	iPrOH/H_2O (v/v = 1:1)	K_2CO_3	RT	1	98
9[a]	EtOH/H_2O (v/v = 1:1)	K_2CO_3	RT	1	97
10[a]	EtOH/H_2O (v/v = 1:8)	K_2CO_3	RT	1	42
11[a]	EtOH/H_2O (v/v = 1:4)	K_2CO_3	RT	1	60
12[a]	EtOH/H_2O (v/v = 1:2)	K_2CO3	RT	1	89
13[a]	EtOH/H_2O (v/v = 1:1)	K_2CO_3	RT	1	97

RT: room temperature.
[a] Reaction conditions: *p*-bromoanisole (2.0 mmol), phenylboronic acid (2.2 mmol), K_2CO_3 (6 mmol), 3.1 wt.% Pd-M-T-S (0.1 mol% Pd) in 20 mL solvent in air.
[b] Yields were determined by GC.

Table 3
Effect of bases on the Suzuki cross-coupling reaction of *p*-bromoanisole and phenylboronic acid

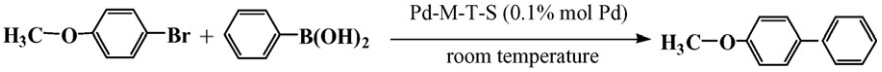

Entry	Base	Yield (%)[b]	Entry	Base	Yield (%)[b]
1[a]	K_2CO_3	97	5[a]	NaOAc	60
2[a]	Na_2CO_3	90	6[a]	NaOEt	98
3[a]	Cs_2CO_3	98	7[a]	Na_3PO_4	81
4[a]	K_3PO_4	86	8[a]	NEt_3	34

[a] Reaction conditions: *p*-bromoanisole (2.0 mmol), phenylboronic acid (2.2 mmol), base (6 mmol), 3.1 wt.% Pd-M-T-S (0.1 mol% Pd) in 20 mL EtOH/H_2O (v/v = 1:1) at RT for 1 h in air.
[b] Yields were determined by GC.

We then examined the effect of bases for the Suzuki reaction. The inorganic bases including K_2CO_3, Cs_2CO_3, Na_2CO_3, K_3PO_4, Na_3PO_4, and NaOEt afforded high yields of 81–98%, as shown in Table 3, entries 1–4, 6, 7. The inorganic base NaOAc, on the other hand, gave a moderate yield of 60%, as illustrated in Table 3, entry 5. However, the organic base NEt_3 gave a lower yield of 34% as shown in Table 3, entry 8. Thus, we select K_2CO_3 as the base and co-solvent EtOH/H_2O (volume ratio = 1:1) as the solvent.

3.3. Catalytic activity of Pd-T-M-S

3.3.1. Test for the catalytic efficiency of Pd-M-T-S

The catalytic efficiency of Pd-M-T-S was also investigated at 50 °C. The catalyst loading contents were decreased from 0.1 mol% to 0.01 mol%, 0.005 mol%, and 0.001 mol% Pd. The desired reaction can then be accomplished with the low-loading content palladium catalyst. The detailed results are listed in Table 4. The turnover frequency (TOF) can reach up to 84,000 h^{-1} with the coupling reaction of *p*-bromoanisole with phenylboronic acid using 0.001 mol% Pd as catalyst. It demonstrated that the Pd-M-T-S sample has been a highly efficient catalyst under mild conditions for the Suzuki reaction.

3.3.2. Suzuki cross-coupling reaction between aryl halide with arylboronic acid

Using our optimized reaction conditions, we now selected a series of aryl bromides and some aryl chlorides in the Suzuki reaction. All reactions were performed using 1:1.1 stoichiometric ratio of aryl halide and arylboronic acid in air. The results are summarized in Table 5. The methodology is applicable to a wide range of aryl bromide substrates (Table 5, entries 1–20); good yields at 87–99% have been obtained under an ambient temperature within a short time with arylboronic acid. A wide range of functional groups has also been tolerated in the reaction. It was similarly demonstrated that the coupling reaction could be efficiently executed at different substituted positions of aryl bromide and of arylboronic acid. Furthermore, sterically hindered aryl bromides could be coupled with phenylboronic acid to give good yields of 87–93% of products (Table 5, entries 5, 6, 10, 11, 15 and 16). Nonetheless, aryl chlorides are not active reactants in our system with a high loading content of 1.0 mol% Pd and give the homo-coupling product for arylboronic acid (Table 5, entries 21–22) as well.

3.3.3. Suzuki cross-coupling reaction between dibromoarenes with arylboronic acids

Palladium-catalyzed Suzuki cross-coupling polymerization has become an extremely useful tool for synthesis of an array of polydisperse conjugated polymers [49]. This method has been likewise applied to the coupling reaction of dibromoarenes with arylboronic acids. Using the abovementioned optimized reaction conditions, the Suzuki cross-coupling reaction has been observed in a variety of aryl bromides including 1,4-dibromobenzene, 1,3-dibromobenzene, 1,2-dibromobenzene and 2,6-dibromopyridine with arylboronic acid. The results are summarized in Table 6. The coupling reaction of 1,4-dibromobenzene, 1,3-dibromobenzene with a variety of arylboronic acid afforded good results, in yields of 93–99% and the ratio of mono-substituted to di-substituted product being 1:99 (Table 6, entries 5–13). The coupling reaction of 1,2-dibromobenzene with a variety of arylboronic acid under ambient temperature also gave relatively good yields of 77–80% (Table 6, entries 1–3) and the good selectivity of a di-substituted product after a long reaction time of 20 h. In contrast, the coupling reaction of 1,2-dibromobenzene with *o*-methoxy phenyl boronic acid gave almost a mono-substituted product and low yield of 15% (Table 6, entry 4). The coupling reaction of 2,6-dibromopyridine with phenyl boronic acid, *p*-methyl phenyl boronic acid, *p*-trifluoromethyl phenyl boronic acid and *m*-methoxy phenyl boronic acid, however, gave good yields of 86–98% (Table 6, entries 14–17). The ratios of mono-substituted and di-substituted product are 5:95, 3:97, 10:90 and 30:70 respectively to phenyl boronic acid, *p*-methyl phenyl boronic acid, *p*-trifluoromethyl phenyl boronic acid and *m*-methoxy phenyl boronic acid (Table 6, entries 14–17). The coupling reaction of 2,6-dibromopyridine with *o*-methoxy phenylboronic acid alternatively gave almost a mono-substituted product and low yield of 32% for a long reaction time of 20 h (Table 6, entry 18). Then again, similar to aryl chlorides, the Suzuki reaction for dichloroarenes gave

Table 4
Efficiency of Pd-M-T-S catalyst on Suzuki reaction of *p*-bromoanisole and phenylboronic acid

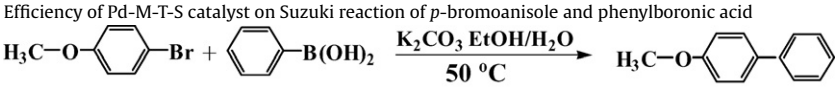

Entry	Pd (mol%)	Time (h)	Yield (%)[b]	TOF (h^{-1})
1[a]	0.1	0.5	99	1,980
2[a]	0.01	0.5	99	19,800
3[a]	0.005	0.5	96	38,400
4[a]	0.001	1	84	84,000

[a] Reaction conditions: *p*-bromoanisole (20 mmol), phenylboronic acid (22 mmol), K_2CO_3 (60 mmol), 3.1 wt.% Pd-M-T-S catalyst in 100 mL EtOH/H_2O (v/v = 1:1) in air.
[b] Yields were determined by GC.

Table 5
Suzuki cross-coupling reaction of aryl halide with arylboronic acids

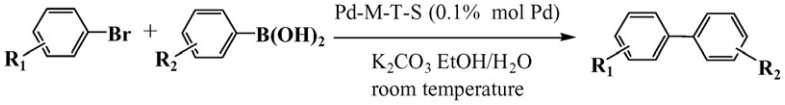

Entry	X	R_1	R_2	Time (h)	Yield (%)[b]	TON
1[a]	Br	*p*-CH_3CO	H	0.5	99	990
2[a]	Br	*p*-CH_3O	H	1	96	960
3[a]	Br	*p*-CH_3	H	1	98	980
4[a]	Br	*p*-OH	H	1	91	910
5[a]	Br	*o*-CH_3O	H	1	87	870
6[a]	Br	*o*-CH_3	H	1	90	900
7[a]	Br	*p*-CH_3CO	*p*-CH_3	0.5	99	990
8[a]	Br	*p*-CH_3O	*p*-CH_3	1	98	980
9[a]	Br	*p*-CH_3	*p*-CH_3	1	98	980
10[a]	Br	*o*-CH_3O	*p*-CH_3	1	91	910
11[a]	Br	*o*-CH_3	*p*-CH_3	1	92	920
12[a]	Br	*p*-CH_3CO	*m*-CH_3O	0.5	98	980
13[a]	Br	*p*-CH_3O	*m*-CH_3O	1	95	950
14[a]	Br	*p*-CH_3	*m*-CH_3O	1	95	950
15[a]	Br	*o*-CH_3O	*m*-CH_3O	1	90	900
16[a]	Br	*o*-CH_3	*m*-CH_3O	1	93	930
17[a]	Br	*p*-CH_3CO	*o*-CH_3O	0.5	96	960
18[a]	Br	*p*-CH_3O	*o*-CH_3O	1	90	900
19[a]	Br	*p*-CH_3	*o*-CH_3O	1	93	930
20[a]	Br	H	*o*-CH_3O	1	96	960
21[c]	Cl	*p*-CHO	H	24	13[d]	–
22[c]	Cl	*p*-CH_3O	H	24	5[d]	–

[a] Reaction conditions: aryl bromides (2.0 mmol), phenylboronic acid (2.2 mmol), K_2CO_3 (6 mmol), 3.1 wt.% Pd-M-T-S (0.1 mol% Pd) in 20 mL EtOH/H_2O (v/v = 1:1) at RT in air.
[b] Yields were determined by GC.
[c] Catalyst (1 mol% Pd).
[d] Yield for homecoupling product of phenylboronic acid.

only a homo-coupling product of arylboronic acid; the results are not shown in the paper.

3.3.4. Reusability

At this point, the recycling ability of Pd-M-T-S was investigated. The coupling reaction of *p*-bromoanisole with phenylboronic acid was chosen as the model reaction. The amount of palladium in the Suzuki coupling reaction was set at a fixed value (Pd/*p*-bromoanisole = 1/1000). Detailed results are listed in Table 7. The reaction time had been extended to 3 h in runs 2–3 for the recycle test. The yields are 96%, 95% and 89%, respectively to run 1, run 2 and run 3. When the reacting time of 3 h was further prolonged to

Table 6
Suzuki cross-coupling reaction of dibromoarenes with arylboronic acids

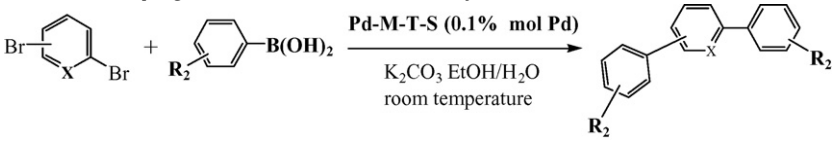

Entry	Dibromoarenes	R_2	Time (h)	Yield (%)[b]	Mono:Di[c]
1[a]	1,2-Dibromobenzene	*p*-Me	20	80	<1:>99
2[a]	1,2-Dibromobenzene	*p*-CF_3	20	60	<1:>99
3[a]	1,2-Dibromobenzene	*m*-CH_3O	20	77	<1:>99
4[a]	1,2-Dibromobenzene	*o*-CH_3O	20	15	>99:<1
5[a]	1,3-Dibromobenzene	H	2	98	<1:>99
6[a]	1,3-Dibromobenzene	*p*-Me	2	99	<1:>99
7[a]	1,3-Dibromobenzene	*p*-CF_3	2	99	<1:>99
8[a]	1,3-Dibromobenzene	*m*-CH_3O	2	98	<1:>99
9[a]	1,4-Dibromobenzene	H	2	99	<1:>99
10[a]	1,4-Dibromobenzene	*p*-Me	2	96	<1:>99
11[a]	1,4-Dibromobenzene	*p*-CF_3	2	98	<1:>99
12[a]	1,4-Dibromobenzene	*m*-CH_3O	2	98	<1:>99
13[a]	1,4-Dibromobenzene	*o*-CH_3O	2	93	<1:>99
14[a]	2,6-Dibromopyridine	H	5	96	5:95
15[a]	2,6-Dibromopyridine	*p*-Me	5	95	3:97
16[a]	2,6-Dibromopyridine	*p*-CF_3	5	98	10:90
17[a]	2,6-Dibromopyridine	*m*-CH_3O	5	86	30:70
18[a]	2,6-Dibromopyridine	*o*-CH_3O	20	32	>99:<1

[a] Reaction conditions: dibromoarenes (1.0 mmol), arylboronic acids (2.5 mmol), K_2CO_3 (6 mmol), catalyst (0.2 mol% Pd) in 20 mL EtOH/H_2O (v/v = 1:1) at RT in air.
[b] Yields were determined by ^1H NMR spectroscopy.
[c] The ratios of mono-substituted to di-substituted product.

Table 7
Reusability of 3.1 wt.% Pd-M-T-S for Suzuki reaction between *p*-bromoanisole and phenylboronic acid

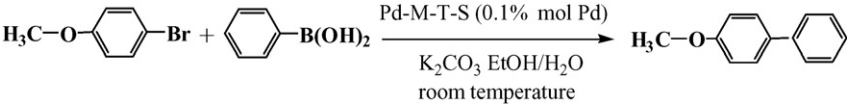

No. of Run[a]	Run 1	Run 2	Run 3	Run 4		Run 5	Run 6
React time (h)	1	3	3	3	12	12	12
Yield (%)[b]	96	95	89	60	90	78	60
Pd content (%)[c]	3	3	2.8	2.8		2.7	2.5

[a] Reaction conditions: *p*-bromoanisole (20 mmol), phenylboronic acid (22 mmol), base (60 mmol), 3.1 wt.% Pd-M-T-S (0.1 mol% Pd) in 100 mL EtOH/H_2O (v/v = 1:1) at RT in air.
[b] Yields were determined by GC.
[c] Pd contents of the fresh and recovered Pd-M-T-S were determined by ICP-AES elemental analysis.

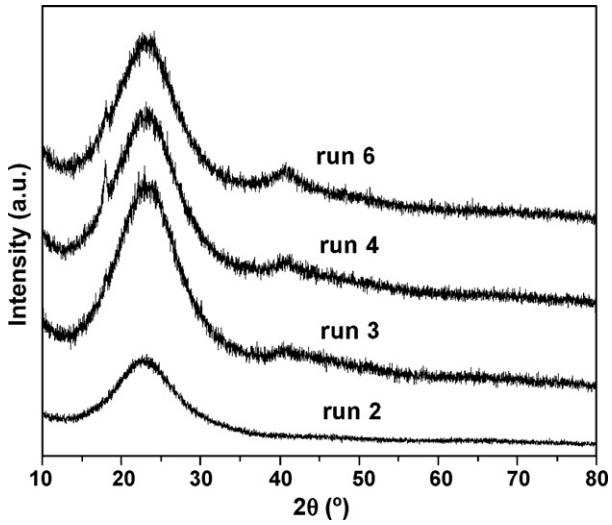

Fig. 8. XRD patterns of recovered Pd-M-T-S after run 2, 3, 4, 6 for the Suzuki reaction in the wide angle ranges.

12 h, the 60% yield was increased to 90% for run 4. The yields are 78% and 60%, respectively, for run 5 and run 6 within 12 h for the recycle experiment. Interestingly, the prepared catalyst was reused for three times with little loss of activity in the reaction. The further recycling experiment will take more time than the previous runs. The activity of Pd-M-T-S catalyst has been subsequently reduced smoothly.

After recycle run of Pd-M-T-S, the contents of palladium in the recovered Pd-M-T-S were confirmed finally by ICP-AES elemental analysis. The weight percentages of palladium are 3.0 wt.%, 3.0 wt.% 2.8 wt.%, 2.8 wt.% 2.7 wt.%, 2.5 wt.% for run 1–6, respectively. The leaching of active palladium species can be identified by the above results of elemental analysis. Wide-angle XRD patterns for the recovered Pd-M-T-S (Table 7, run 2, 3, 4, 6) have presented in the Fig. 8. The peaks of palladium crystalline structure were found in the wide-angle XRD patterns of run 3, 4, 6 for the recovered Pd-M-T-S (Fig. 8).

3.4. Comparison of performance of Pd-M-T-S catalyst with Pd (II)/SBA-15 and $PdCl_2$ for Suzuki reaction at room temperature

Using our optimized reaction conditions, we now compared the performance of Pd-M-T-S with Pd (II)/SBA-15 and $PdCl_2$ for the Suzuki cross-coupling reaction between *p*-bromoanisole and phenylboronic acid at room temperature. The amount of palladium in the Suzuki coupling reaction was also set at the previously mentioned value (Pd/*p*-bromoanisole = 1/1000 in molar ratio). The detailed results are listed in Table 8. The supported catalyst of Pd (II)/SBA-15 correspondingly gave a high yield of 93% in 1 h (Table 8, entry 2). The homogeneous catalyst of $PdCl_2$ gave high yield of 95% in 1 h (Table 7, entry 3). After Suzuki reaction, the contents of palladium in the recovered Pd-M-T-S and the recovered Pd (II)/SBA-15 were confirmed finally by ICP-AES elemental analysis. The weight percentages of palladium are 3.0 wt.%, 1.6 wt.% for the recovered Pd-M-T-S and the recovered Pd (II)/SBA-15 respectively. Combining above results with the results of the recycle test, we can conclude that the benefit of these imidazolium-silica composites can prevent leaching of Pd salts to a degree during Suzuki reactions. The wide-angle XRD patterns for the recovered Pd-M-T-S and the recovered Pd (II)/SBA-15 have presented in the Fig. 9 respectively. The new peak at 40° in Fig. 9b is the peak of palladium crystalline structure and that was not found in Fig. 9a.

3.5. Structural and mechanism studies of the Pd-M-T-S catalyst

Andrews et al. developed a possible mechanism for catalyst formation, in which the true catalyst was possibly reduced to Pd (0) nanoclusters or molecular, “naked” Pd species [20], when they introduced Pd (II)-exchanged perovskites as pre-catalysts in the Suzuki coupling reaction of bromoarenes and arylboronic acids.

Palladium catalysts can be highly dispersed in our supporting material due to electrostatic interaction, owing to the presence of

Table 8
Comparison of performance of Pd-M-T-S catalyst with Pd (II)/SBA-15 and $PdCl_2$ for Suzuki reaction at room temperature

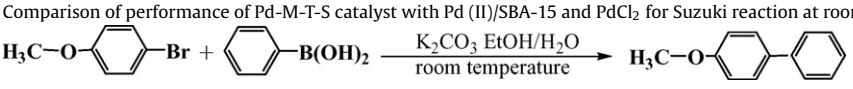

Entry	Pd catalyst	Pd (mol%)	Yield[b]	Pd content (%)[c]
1[a]	Pd-M-T-S	0.1	96	3
2[a]	Pd (II)/SBA-15	0.1	93	1.6
3[a]	$PdCl_2$	0.1	95	–

[a] Reaction conditions: *p*-bromoanisole (20 mmol), phenylboronic acid (22 mmol), base (60 mmol), in 100 mL EtOH/H_2O (v/v = 1:1) at RT for 1 h in air.
[b] Yields were determined by GC.
[c] Pd contents of the recovered Pd-M-T-S and the recovered Pd (II)/SBA-15 were determined by ICP-AES elemental analysis.

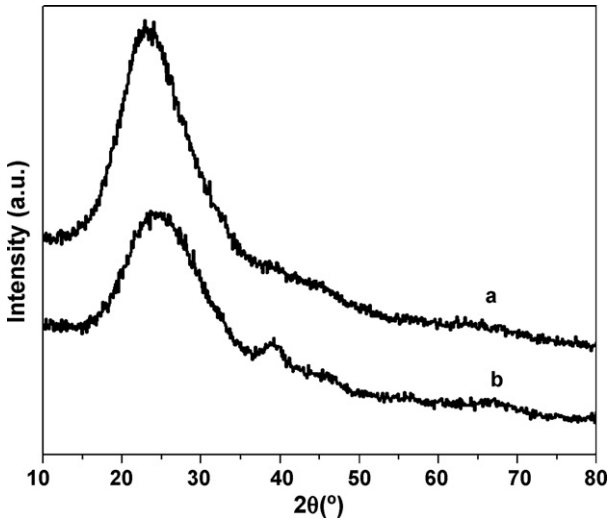

Fig. 9. XRD patterns of recovered Pd-M-T-S after first run for the Suzuki reaction (a) and recovering Pd (II)/SBA-15 after reaction (b) in the wide angle ranges.

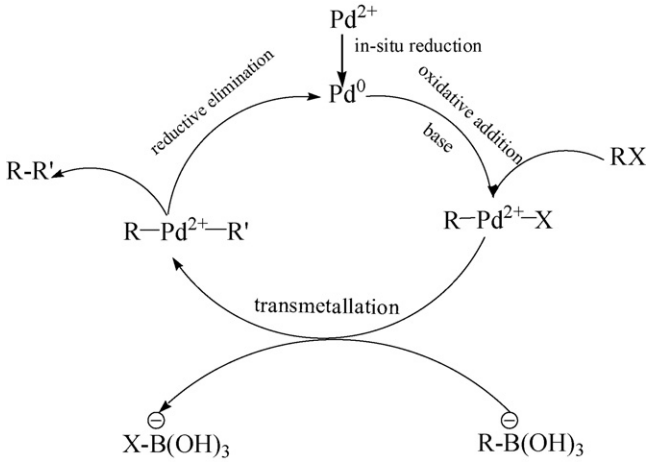

Fig. 11. Catalytic cycle of Pd-M-T-S for the Suzuki coupling reaction.

imidazolium salts on the pore walls. Once the reaction is starting, the color of Pd-M-T-S changes to black in the reaction mixture. It suggests that Pd (II) on Pd-M-T-S has been in situ reduced to zero valence palladium during the Suzuki reaction. As shown in Fig. 10, the binding energies of Pd $3d_{5/2}$ is shifted from 336.5 eV for fresh Pd-M-T-S to 335.1 eV for recovered Pd-M-T-S in Table 6, run 1. This indicates that the valence state of palladium have transformed from bivalence into zero valence completely after the Suzuki reaction [50]. Therefore, we assume that ligand-free palladium (II) has been reduced in situ to zero valence palladium and has entered into the catalytic cycle (Fig. 11).

It is widely believed that during the catalytic cycle, the Pd (II) complexes initially presented in the catalyst are reduced to Pd (0) species, and unsaturated Pd (0) complexes can interact strongly with each other under the reaction condition to form Pd clusters. The Pd (0) species is subject to two competing processes. The catalyst can either enter the catalytic cycle or aggregate to form initially soluble palladium clusters, which at some point will turn into insoluble palladium black. The latter process is self-catalyzed and rapidly leads to the withdrawal of all palladium from the catalytic cycle. The catalyst loading contents is low, and so the actual concentration of active catalytic species in solution is below levels that promote self-deactivation [51]. Therefore, the low-loading contents (0.001 mol% Pd) of Pd-M-T-S (Table 4, entry 4) gave higher catalytic efficiency. Narayanan and El-Sayed found that colloidal metal nanoparticles are unstable and undergo changes in their morphology (size and shape) to survive in the reaction mixture [52]. They also observed that the spherical PVP–palladium nanoparticles grew larger after the first cycle of the Suzuki reaction because of the Ostwald ripening process. They then explored the possibility of using carbon-supported metal nanoparticles as good potential catalysts to catalyze the Suzuki reaction [21]. In general, the catalytic activity of palladium nanoparticles is inversely proportional to the size of palladium nanoparticles. Primary agglomeration of active palladium species form larger palladium nanoparticles. However, the presence of the support makes the palladium nanoparticles resistant to aggregation, precipitation and also preserves their catalytic activity. Therefore, the long term stability of the immobilized catalyst would be related to the ability of the support to release and catch the active species in order to regenerate the catalyst for a new Suzuki reaction cycle.

Forsyth et al. evaluated a variety of ligand-free catalysts including $Pd(OAc)_2$, $PdCl_2$ and Pd/C in both ionic liquid media and NMP [53]. They found a better catalytic performance in the ionic liquid and decreased palladium black formation using palladium salts as pre-catalysts. Ammonium salts for homogeneous catalysts have shown related sequestration and stabilization effects for palladium species. Our highly dispersed palladium supported catalyst was prepared through electrostatic interaction of the imidazolium salts into the mesoporous silica. As shown in Fig. 11, ligand-free palladium (II) is reduced in situ to zero valence palladium and enters into the reacting cycle (oxidative-addition, transmetallation and reductive elimination). At the end of the reaction, palladium (0) is re-deposited on the pore walls. With the pore-containing effect of mesoporous silica and stabilized imidazulium salt on the inner walls, the palladium (0) did not simply agglomerate. Comparison

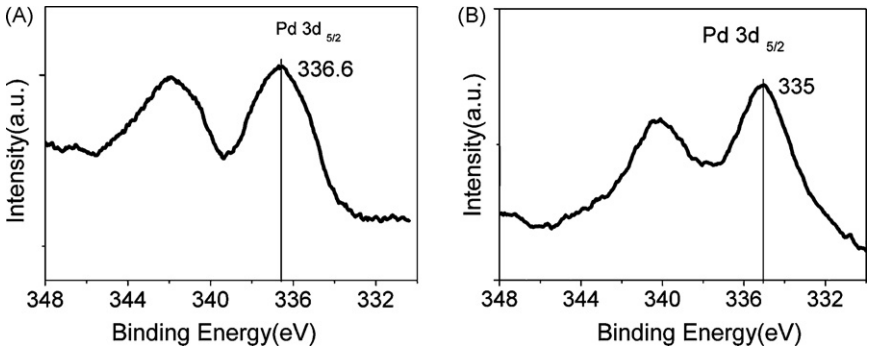

Fig. 10. XPS spectra of Pd-M-T-S before (A) and after (B) reaction.

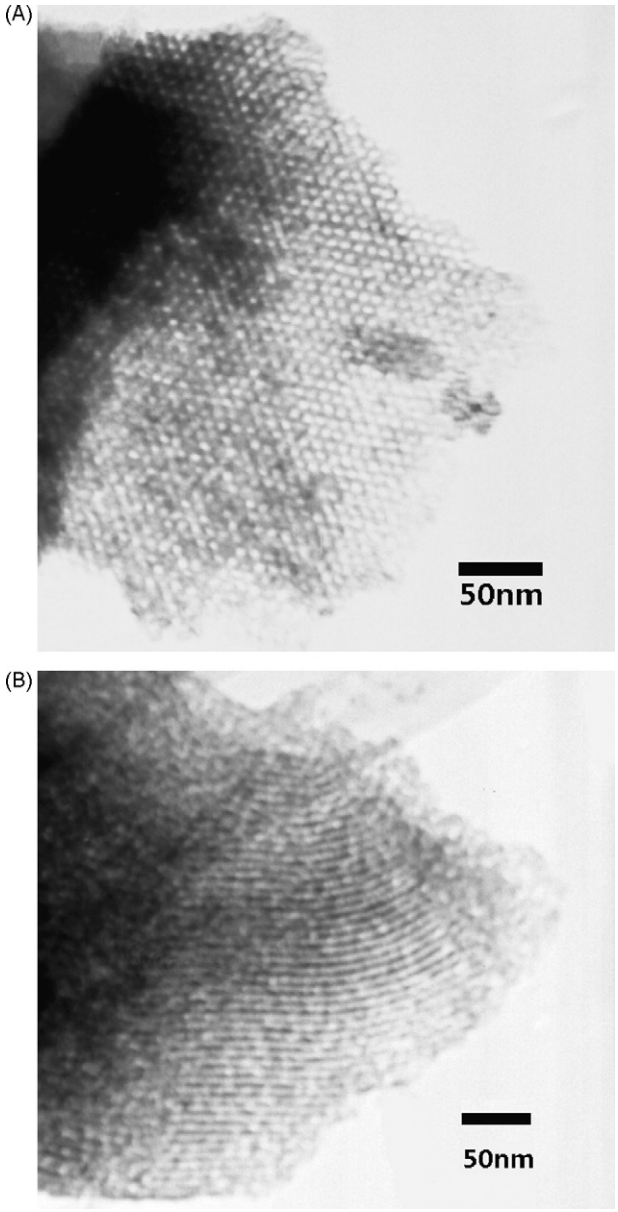

Fig. 12. TEM images of recovered Pd-M-T-S after first run for the Suzuki reaction, (A) micrograph taken with the beam direction parallel to the pore, (B) micrograph taken with the beam direction perpendicular to the pore.

of the wide-angle XRD patterns of recovered Pd-M-T-S and recovered Pd (II)/SBA-15 (Figs. 8 and 9) have demonstrated that the peak of palladium crystalline structure cannot be found in recovered Pd-M-T-S at run 1 and 2 (Figs. 8 and 9). The peak of palladium crystalline structure can be found in Fig. 8 afterwards run 3. On the XRD patterns of recovered Pd (II)/SBA-15 (Fig. 9b), the peak of palladium crystalline structure can be found after the first run reaction. Imidazolium salts-functionalized mesoporous silica SBA-15 can capture and stabilize catalytically active soluble palladium species, which are generated during the Suzuki reaction. Therefore, the palladium-imidazolium-silica composites (Pd-M-T-S) is superior in the long term stability to the control SBA-15/palladium samples (Pd (II)/SBA-15). As shown in TEM images in Fig. 12, there is no visible palladium nanoparticles on the imidazolium-silica support. Combining the XRD patterns (Figs. 8 and 9) with TEM images (Fig. 12) for the recovered palladium-imidazolium-silica composites (Pd-M-T-S), palladium (0) can disperse very well after the Suzuki reaction for Pd-M-T-S. Similarly, agglomeration of palladium can be controlled due to the stabilizing effect of the imidazulium salt contained on the mesoporous silica inner walls. The catalytic activity for palladium can be retained to some extent.

4. Conclusions

We have successfully prepared highly dispersed palladium supported catalysts in that palladium salts are loaded in the pore channels of imidazolium salts-functionalized mesoporous silica SBA-15 due to electrostatic interaction. It has demonstrated a highly efficient recyclable catalyst for the room-temperature Suzuki coupling of a wide range of aryl bromides and dibromoarenes with arylboronic acids. Controlling supported palladium salts located in the inner pore channel can effectively restrain palladium agglomeration to form lager palladium particles in the reaction owing to the pore containment effect of silica and the stabilization of imidazolium salts on the inner walls synergistically.

Acknowledgements

We are grateful for the support from the National Natural Science Foundation of China (Creative Research Group: 50621302), High-tech “863” Project (2006AA03Z224) and “973” Project (2006CB708601) of Ministry of Science and Technology of China, the Distinguished Young Fund of Jilin Province (20050104), the International Collaboration Project (20050702-2) and Project (20060505) from Department of Science and Technology, Jilin Province, China.

References

[1] J. Tsuji (Ed.), Palladium Reagents and Catalysts—New Perspectives for the 21st Century, Wiley-VCH, New York, 2004, pp. 1–6.
[2] R.F. Heck, J.P. Nolley, J. Org. Chem. 37 (1972) 2320–2322.
[3] R.F. Heck, Acc. Chem. Res. 12 (1979) 146–151.
[4] N. Miyaura, A. Suzuki, Chem. Rev. 95 (1995) 2457–2483.
[5] A. Suzuki, Chem. Commun. (2005) 4759–4763.
[6] K. Sonogashira, Y. Tohda, N. Hagihara, Tetrahedron Lett. (1975) 4467–4470.
[7] J.K. Stille, Angew. Chem. Int. Ed. 25 (1986) 508–524.
[8] A.S. Guram, R.A. Rennels, S.L. Buchwald, Angew. Chem. Int. Ed. 34 (1995) 1348–1350.
[9] J. Louie, J.F. Hartwig, Tetrahedron Lett. (1995) 3609–3612.
[10] C. Dai, G.C. Fu, J. Am. Chem. Soc. 123 (2001) 2719–2724.
[11] T.E. Barder, S.D. Walker, J.R. Martinelli, S.L. Buchwald, J. Am. Chem. Soc. 127 (2005) 4685–4696.
[12] W.A. Herrmann, Angew. Chem. Int. Ed. 41 (2002) 1290–1309.
[13] O. Navarro, R.A. Kelly, S.P. Nolan, J. Am. Chem. Soc. 125 (2003) 16194–16195.
[14] W.A. Herrmann, C. Brossmer, K. Ofele, C.P. Reisinger, T. Priermeier, M. Beller, H. Fischer, Angew. Chem. Int. Ed. 34 (1995) 1844–1848.
[15] D. Dallinger, C.O. Kappe, Chem. Rev. 107 (2007) 2563–2591.
[16] L. Yin, J. Liebscher, Chem. Rev. 107 (2007) 133–173.
[17] D.J. Cole-Hamilton, R.P. Tooze (Eds.), Catalysis by Metal Complexes, Volume 30: Catalyst Separation, Recovery and Recycling, Springer, Netherlands, 2006, pp. 9–17.
[18] K. Shimizu, R. Maruyama, S. Komai, T. Kodama, Y. Kitayama, J. Catal. 227 (2004) 202–209.
[19] H. Bulut, L. Artok, S. Yilmaz, Tetrahedron Lett. 44 (2003) 289–291.
[20] S.P. Andrews, A.F. Stepan, H. Tanaka, S.V. Ley, M.D. Smith, Adv. Synth. Catal. 347 (2005) 647–654.
[21] R. Narayanan, M.A. El-Sayed, J. Catal. 234 (2005) 348–355.
[22] T. Maegawa, Y. Kitamura, S. Sako, T. Udzu, A. Sakurai, A. Tanaka, Y. Kobayashi, K. Endo, U. Bora, T. Kurita, A. Kozaki, Y. Monguchi, H. Sajiki, Chem. Eur. J. 13 (2007) 5937–5943.
[23] K. Mori, K. Yamaguchi, T. Hara, T. Mizugaki, K. Ebitani, K. Kaneda, J. Am. Chem. Soc. 124 (2002) 11572–11573.
[24] A. Desforges, R. Backov, H. Deleuze, O. Mondain-Momval, Adv. Funct. Mater. 15 (2005) 1689–1695.
[25] K. Okamoto, R. Akiyama, H. Yoshida, T. Yoshida, S. Kobayashi, J. Am. Chem. Soc. 127 (2005) 2125–2135.
[26] C.M. Crudden, M. Sateesh, R. Lewis, J. Am. Chem. Soc. 127 (2005) 10045–10050.
[27] A. Corma, D. Das, H. García, A. Leyva, J. Catal. 229 (2005) 322–331.
[28] K. Shimizu, S. Koizumi, T. Hatamachi, H. Yoshida, S. Komai, T. Kodama, Y. Kitayama, J. Catal. 228 (2004) 141–151.
[29] D.D. Das, A. Sayari, J. Catal. 246 (2007) 60–65.

[30] P. Han, X. Wang, X. Qiu, X. Ji, L. Gao, J. Mol. Catal. A: Chem. 272 (2007) 136–141.
[31] C.L. Deng, S.M. Guo, Y.X. Xie, J.H. Li, Eur. J. Org. Chem. (2007) 1457–1462.
[32] J. Dupont, R.F. de Souza, P.A.Z. Suarez, Chem. Rev. 102 (2002) 3667–3692.
[33] J.P. Mikkola, P. Virtanen, H. Karhu, T. Salmi, D.Y. Murzin, Green Chem. 8 (2006) 197–205.
[34] P. Migowski, J. Dupont, Chem. Eur. J. 13 (2007) 32–39.
[35] C.P. Mehnert, Chem. Eur. J. 11 (2005) 50–56.
[36] A. Riisager, R. Fehrmann, M. Haumann, P. Wasserscheid, Top. Catal. 40 (2006) 91–102.
[37] D.W. Kim, D.Y. Chi, Angew. Chem. Int. Ed. 43 (2004) 483–485.
[38] C.E. Song, M.Y. Yoon, D.S. Choi, Bull. Korean Chem. Soc. 26 (2005) 1321–1330.
[39] C. Zhong, T. Sasaki, M. Tada, Y. Iwasawa, J. Catal. 242 (2006) 357–364.
[40] K. Yamaguchi, C. Yoshida, S. Uchida, N. Mizuno, J. Am. Chem. Soc. 127 (2005) 530–531.
[41] M. Gruttadauria, S. Riela, C. Aprile, P.L. Meo, F. D'Anna, R. Noto, Adv. Synth. Catal. 348 (2006) 82–92.
[42] H. Hagiwara, K.H. Ko, T. Hoshib, T. Suzuki, Chem. Commun. (2007) 2838–2840.
[43] J.H. Clark, D.J. Macquarrie, S.J. Tavener, Dalton Trans. (2006) 4297–4309.
[44] A. Taguchi, F. Schüth, Microporous Mesoporous Mater. 77 (2005) 1–45.
[45] C. Thiot, M. Schmutz, A. Wagner, C. Mioskowski, Angew. Chem. Int. Ed. 45 (2006) 2868–2871.
[46] D. Zhao, Q. Huo, J. Feng, B.F. Chmelka, G.D. Stucky, J. Am. Chem. Soc. 120 (1998) 6024–6036.
[47] H. Chen, S. Huh, J.W. Wiench, M. Pruski, V.S.Y. Lin, J. Am. Chem. Soc. 127 (2005) 13305–13311.
[48] X. Ji, Q. Hu, J.E. Hampsey, X. Qiu, L. Gao, J. He, Y. Lu, Chem. Mater. 18 (2006) 2265–2274.
[49] A. de Meijere, F. Diederich (Eds.), Metal-Catalyzed Cross-Coupling Reactions, 2nd ed., Wiley-VCH, New York, 2004, pp. 41–107.
[50] K.R. Priolkar, P. Bera, P.R. Sarode, M.S. Hegde, S. Emura, R. Kumashiro, N.P. Lalla, Chem. Mater. 14 (2002) 2120–2128.
[51] A.H.M. de Vries, J. Mulders, J.H.M. Mommers, H.J.W. Henderickx, J.G. de Vries, Org. Lett. 5 (2003) 3285–3288.
[52] R. Narayanan, M.A. El-Sayed, J. Am. Chem. Soc. 125 (2003) 8340–8347.
[53] S.A. Forsyth, H.Q.N. Gunaratne, C. Hardacre, A. McKeown, D.W. Rooney, K.R. Seddon, J. Mol. Catal. A: Chem. 231 (2005) 61–66.